Metal to marginal-metal transition in two-dimensional ferromagnetic electron gases

Weiwei Chen,[1] C. Wang,[2,3,*] Qinwei Shi,[1] Qunxiang Li,[1] and X. R. Wang[4,5,†]

[1]*Hefei National Laboratory for Physical Sciences at the Microscale and Synergetic Innovation Center of Quantum Information and Quantum Physics, University of Science and Technology of China, Hefei, Anhui 230026, China*

[2]*Center for Joint Quantum Studies and Department of Physics, School of Science, Tianjin University, Tianjin 300350, China*

[3]*School of Electronic Science and Engineering and State Key Laboratory of Electronic Thin Films and Integrated Devices, University of Electronic Science and Technology of China, Chengdu 610054, China*

[4]*Department of Physics, The Hong Kong University of Science and Technology, Clear Water Bay, Kowloon, Hong Kong*

[5]*Shenzhen Research Institute, The Hong Kong University of Science and Technology, Shenzhen 518057, China*

(Received 5 July 2019; revised manuscript received 8 November 2019; published 3 December 2019)

Two-dimensional ferromagnetic electron gases subject to random scalar potentials and Rashba spin-orbit interactions exhibit a striking quantum criticality. As disorder strength W increases, such a system undergoes two transitions. It first changes from a normal diffusive metal consisting of extended states to a marginal metal consisting of critical states at a critical disorder $W_{c,1}$. Another transition from the marginal metal to an insulator occurs at a stronger disorder $W_{c,2}$. Through highly accurate numerical procedures based on the recursive Green's function and the exact diagonalization methods, we elucidate the nature of the quantum criticality and the properties of the pertinent states. The conductance is described by an unorthodox one-parameter scaling law: Conductance of various system sizes and disorders collapse into two branches of a scaling curve corresponding to diffusive metal and insulating phases with an exponentially diverging correlation length, $\xi \propto \exp[\alpha/\sqrt{|W - W_c|}]$, near transition points. Finite-size scaling analysis of the inverse participation ratio reveals that the states of the marginal metal are fractals of a universal fractal dimension $D = 1.90 \pm 0.02$, while those of the diffusive metal spread over the whole system with $D = 2$ and states in the insulating phase are localized with $D = 0$. The phase diagram for diffusive metals, marginal metals, and the Anderson insulators is plotted in the disorder-magnetic-coupling plane.

DOI: 10.1103/PhysRevB.100.214201

I. INTRODUCTION

Anderson localization is a long-lasting fundamental concept in condensed-matter physics [1–9] and keeps bringing us surprises, especially at the critical dimensionality of 2 [10–12]. In very early times, the orthodox view was the absence of diffusion of an initially localized wave packet at an arbitrarily weak disorder in one- and two-dimensional electron gases (2DEGs) while metallic states and Anderson localization transitions (ALTs) can occur in three dimensions [13,14]. Later, more careful renormalization group calculations [15] and numerical simulations [16–20], together with experiments [11], showed that intrinsic degrees of freedom can alter the results in two dimensions: Half-integer spin particle systems support ALTs when the spin rotational symmetry is broken through spin-orbit interactions (SOIs), regardless of whether the time-reversal symmetry is preserved [Gaussian symplectic ensembles (GSEs)] [15–20] or not [Gaussian unitary ensembles (GUEs)] [21–23]. The surest examples are probably of both noninteracting [24–26] and interacting [27,28] 2DEGs in strong perpendicular magnetic fields (quantum Hall systems). On the other hand, all states of disordered noninteracting integer-spin particle systems must be localized [29,30].

However, recent numerical studies [21–23,31–34] showed that the current understanding of ALTs in noninteracting 2DEGs is far from completed when SOIs are involved. For example, in contrast to the predictions based on the nonlinear σ model that claim only localized states exist in the GUEs [15], a band of extended states together with an ALT or a Kosterlitz-Thouless (KT)-type transition can exist in 2DEGs without time-reversal symmetry, depending on the form of SOIs and the strength of magnetic field [21–23]. In this work, we observe a phase transition from a normal metal to a *marginal metal* [35], consisting of a band of critical states, in a ferromagnetic 2DEG on a square lattice subject to a Rashba SOI and random on-site potentials. The results are obtained from the finite-size scaling analysis of two-terminal conductances and the inverse participation ratio (IPR) analysis of wave functions obtained from the exact diagonalization method. The marginal-metal (MM) phase exists between a diffusive-metal (DM) phase at weak disorders and an Anderson insulator (AI) phase at strong disorders. Scaling analyses of IPRs show wave functions of states in the MMs of fractals of dimension $D = 1.90 \pm 0.02$, a feature reminiscent of a band of critical states in the random SU(2) model subject to strong magnetic fields [21].

Our main result is a marginal-metal phase whose β function (symbols and the black line in Fig. 1), defined as $\beta(\ln g_L) = d \ln g_L / d \ln L$, vanishes. For a comparison, β of other types of phase transitions in two dimensions are

*Corresponding author: physcwang@tju.edu.cn
†Corresponding author: phxwan@ust.hk

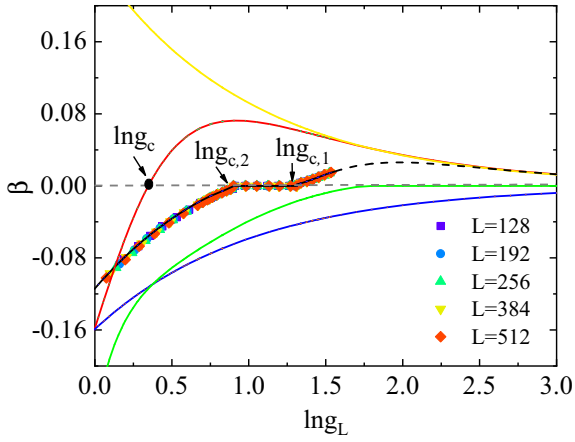

FIG. 1. $\beta(\ln g_L)$ of various 2D systems. The black solid line is the result of current work (different symbols for different system sizes). The black dashed line is plotted according to an analytical formula [15] (illustrated in the Appendix). For noninteracting Schrödinger electrons, no delocalization-localization transition is allowed for the Gaussian orthogonal ensembles (GOEs; the blue line) [11,12], where time-reversal and spin-rotation symmetries are preserved. For the GSEs [16–20,36], there is one $\beta = 0$ point (the red line), corresponding to an unstable fixed point in renormalization group flow. The KT transition (the green line) from a band of critical states to localized states can also exist [21]. For a Dirac Hamiltonian, numerical simulations suggest all states are extended in single-valley graphenes [37] (the yellow line), while KT transitions are also allowed if random fluxes [31] or intervalley scatterings [35,38] exist.

also sketched. Here g_L and L are dimensionless conductance and system size, respectively. Positive β for $g_L > g_{c,1}$ corresponds to a metallic phase, while negative β for $g_L < g_{c,2}$ corresponds to an insulating phase. Between the two critical conductances $g_{c,1}$ and $g_{c,2}$, $\beta = 0$ describes a MM phase. Different from an ALT that occurs at a fixed point [16–20,22,23], the MM phase between $[g_{c,1}, g_{c,2}]$ is a fixed line on which the conductance does not change as system size is uniformly scaled. Furthermore, near both DM-MM and MM-AI transition points, correlation lengths ξ in both DM and AI phases diverge exponentially with W at the transition point W_c, $\xi(W) \propto \exp[\alpha/\sqrt{|W - W_c|}]$, similar to that in a KT transition (the green line) [21,31,35].

This paper is organized as follows. The model and numerical methods are described in Sec. II. Various results are presented in Secs. III and IV. A summary is given in Sec. V.

II. MODEL AND METHODS

Our model is a tight-binding Hamiltonian on a square lattice of size L^2 and unit lattice constant,

$$H = \sum_i c_i^\dagger \epsilon_i c_i - \sum_{\langle i,j \rangle} c_i^\dagger R_{ij} c_j, \tag{1}$$

where $c_i^\dagger = (c_{i,\uparrow}^\dagger, c_{i,\downarrow}^\dagger)$ and c_i are, respectively, the single-electron creation and annihilation operators on site $i = (x_i, y_i)$, with x_i, y_i being integers and $1 \leqslant x_i, y_i \leqslant L$. Here $\langle ij \rangle$ denotes i and j as the nearest-neighbor sites. The first term describes on-site energy with both spin-independent and spin-dependent contributions,

$$\epsilon_i = \epsilon_0 \sigma_0 - \Delta \sigma_z + V_i \sigma_0, \tag{2}$$

where σ_0 and $\sigma_{x,y,z}$ are the 2×2 identity and the Pauli matrices, respectively. ϵ_0 is the constant energy, and spin-independent V_i is the uncorrelated random energy on site i that follows the normal distribution of zero mean and the variance of W^2. W therefore measures the degree of randomness. $-\Delta\sigma_z$ is a ferromagnetic term that breaks the time-reversal symmetry, and Δ measures the exchange splitting [39]. A Rashba SOI is encoded in the hopping matrices R_{ij}, parameterized by matrices R_x and R_y along the x and y directions, respectively,

$$R_x = \tfrac{1}{2}(t\sigma_0 + i\tilde{\alpha}\sigma_y), \quad R_y = \tfrac{1}{2}(t\sigma_0 - i\tilde{\alpha}\sigma_x), \tag{3}$$

where the spin-independent hopping coefficient t can be used as the energy unit and the parameter $\tilde{\alpha}$ measures the strength of SOIs. In the clean limit of $V_i = 0$, model (1) can be blocked diagonalized in the momentum space as $H = \sum_{\boldsymbol{k}} c_{\boldsymbol{k}}^\dagger h(\boldsymbol{k}) c_{\boldsymbol{k}}$, with

$$h(\boldsymbol{k}) = (\epsilon_0 - \cos k_x - \cos k_y)\sigma_0 - \Delta\sigma_z + \tilde{\alpha}(\sin k_x \sigma_y - \sin k_y \sigma_x). \tag{4}$$

Hereafter, we fix $\epsilon_0 = 2$ such that the effective $\boldsymbol{k} \cdot \boldsymbol{p}$ Hamiltonian near the band edge reads $\frac{p^2}{2} + \tilde{\alpha}(\boldsymbol{p} \times \boldsymbol{\sigma}) \cdot \hat{z} - \Delta\sigma_z$. This form of Hamiltonian has been widely employed to enlighten the intrinsic and extrinsic mechanism of the anomalous Hall effect, and possible physical realizations of model (1) include a large family of ferromagnetic semiconductors such as MnGaAs and other III-V host materials [39].

To investigate the localization properties of states of model (1), we use the Landauer formula to calculate the dimensionless conductance of a disordered sample between two clean semi-infinite leads at a given Fermi level E, $\tilde{g}_L = \mathrm{Tr}[TT^\dagger]$, where T is the transmission matrix [40]. To exclude the contribution from contact resistances, we define the dimensionless conductance g_L as $1/g_L = 1/\tilde{g}_L - 1/N_c$, where N_c is the number of propagating modes of the clean sample at Fermi energy E [41]. Different quantum phases are determined by the following criteria: (1) dg_L/dL is positive when the Fermi level is in the DM phase and negative in the insulating phase. $dg_L/dL = 0$ in the MM phase. (2) In the vicinity of phase transition points, the one-parameter scaling hypothesis [13] holds such that $g_L(W, E)$ of different system sizes collapse into a universal smooth curve $f(x)$, i.e.,

$$g_L = f(L/\xi), \tag{5}$$

with the correlation length ξ diverging at the transition points. Since previous numerical studies suggest that the effect of irrelevant variables plays a significant role in the finite-size scaling analysis [42], we will also include the most important irrelevant scaling variable (up to the first order) in our finite-size scaling analysis. Following the method in Ref. [42], Eq. (5) with the irrelevant scaling variable ϕ becomes $g_L = f(L/\xi) + \phi L^y \tilde{f}(L/\xi)$, where $y < 0$ is the exponent for the irrelevant variable. The corrected conductances $g_L^{\mathrm{cor}} = g_L - \phi L^y \tilde{f}(L/\xi)$ are used to obtain the scaling functions.

III. CONDUCTANCE

Two typical examples are shown in Fig. 2(a), which plots g_L as a function of W for $E = 0.2$ (near the band edge), $\tilde{\alpha} = 0.2$, and $\Delta = 0.01$ and 0 (inset). Clearly, in the absence

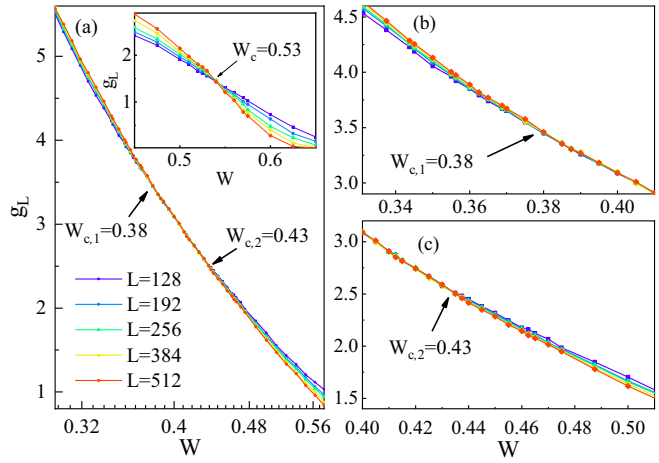

FIG. 2. (a) g_L as a function of W for $L = 128$, 192, 256, 384, and 512 at $E = 0.2$ and $\Delta = 0.01$. The inset is the same plot, but for $\Delta = 0$. (b) Enlargement of the regime near $W_{c,1}$. (c) Same as (b), but for the regime near $W_{c,2}$.

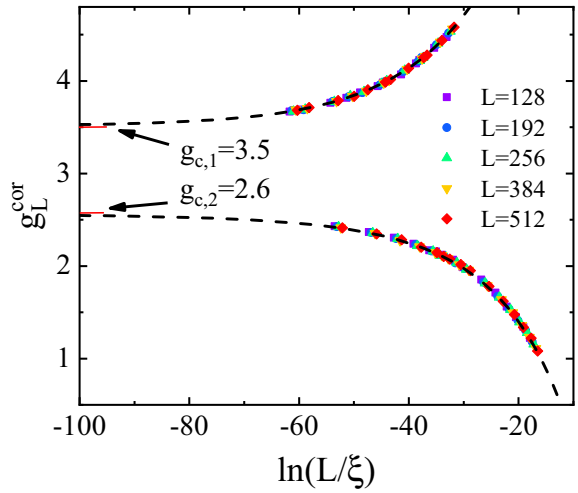

FIG. 3. Scaling functions $f(x = \ln L/\xi)$ in the DM phase ($W < W_{c,1} = 0.38 \pm 0.01$, the upper branch) and in the AI phase ($W > W_{c,2} = 0.43 \pm 0.01$, the lower branch).

of ferromagnetic coupling $\Delta = 0$ when model (1) belongs to the GSE, all curves cross at a single point W_c. dg_L/dL is positive for $W < W_c$ and negative for $W > W_c$. These scaling behaviors are support of an ALT at W_c. Finite-size scaling analysis (elucidated in the Appendix) shows that g_L for different sizes L collapse into a single smooth scaling curve, and ξ diverges as $|E - E_c|^{-\nu}$ with a universal exponent $\nu = 2.8 \pm 0.1$, which is the same as those in the literature [18–20].

Strikingly, once systems enter the GUE by switching on the ferromagnetic coupling, say, $\Delta = 0.01$, we observe a MM phase in the window of $W \in [W_{c,1} = 0.38 \pm 0.01, W_{c,2} = 0.43 \pm 0.01]$ within which $dg_L/dL = 0$ for all L while states for $W < W_{c,1}$ and $W > W_{c,2}$ are extended and localized, respectively. Two phase transitions are evident in Figs. 2(b) and 2(c), which are the enlargements of Fig. 2(a) near $W_{c,1}$ and $W_{c,2}$, respectively. The MM-AI transition at $W_{c,2}$, in addition to the zero plateau of the β function shown in Fig. 1, is highly evocative of the KT criticality arising in another unitary ensemble with random SOIs [21], disordered graphene [35], and 2DEGs with random fluxes [31]. Nonetheless, the DM-MM transition at $W_{c,1}$ from a band of extended states to a band of critical states is highly nontrivial since both of them are of metallic phases in the sense that their wave functions spread over the whole lattice (see Sec. IV).

To substantiate the validity of the one-parameter scaling hypothesis, we show that all curves in Figs. 2(b) and 2(c) collapse into two smooth functions $f(x = \ln L/\xi)$, shown in Fig. 3. These are direct verification of quantum phase transitions at $W_{c,1}$ [$g_L(W_{c,1}) = g_{c,1}$] and $W_{c,2}$ [$g_L(W_{c,2}) = g_{c,2}$]. On the insulating side and near the phase transition point $W_{c,2}$, the correlation length is expected to diverge as $\xi \propto \exp[\alpha_2/\sqrt{|W - W_{c,2}|}]$, with $\alpha_2 = 8 \pm 1$, a fingerprint of the KT transitions [21,31,35]. Differently, there are no reliable analytical and numerical estimates for the divergence law near the DM-MM transition $W_{c,1}$. Scaling analysis also suggests $\xi \propto \exp[\alpha_1/\sqrt{|W - W_{c,1}|}]$, with $\alpha_1 = 9 \pm 4$. We have also carried out the finite-size scaling analysis by assuming only one quantum phase transition point and the power-law-divergent correlation length $\xi \propto |W - W_c|^{-\nu}$ (presented in the Appendix). We found that the critical exponent ν is bigger, by at least one order of magnitude, than any known values in 2DEGs [11,12]. Moreover, ν is not universal and depends on the range of disorders. ν keeps increasing as one approaches the transition point. This is against the renormalization group theory. We thus exclude the single quantum phase transition, and our data support two KT transition points where the correlation length diverges exponentially at the DM-MM transition.

So far, we have provided one example of the DM-MM-AI transition in model (1). Needless to say, many questions arise, and among them, the most important one may be the proof of the universality of such quantum phase transitions. In fact, we have observed the three phases at different Fermi energies and exchange splitting energies with the same diverging ξ, i.e., $\xi \propto \exp[\alpha/\sqrt{|W - W_c|}]$ near critical disorders of W_c and α that are summarized in Tables I and II. The same physics is observed if we choose E as the scaling variable at a fixed disorder. One example is shown in Fig. 4, which depicts g_L as a function of E for $W = 0.4$. Apparently, the MM phase appears between the DM and AI phases and persists in a finite range of energy $E \in [0.19, 0.38]$. Finite-size scaling analysis shows that the correlation lengths $\xi(E)$ diverge as $\xi(E) \propto \exp[\alpha\sqrt{|E - E_c|}]$, with $E_{c,1} = 0.19 \pm 0.03$, $\alpha_1 = 14 \pm 5$ near the DM-MM transition and $E_{c,2} = 0.38 \pm 0.02$, $\alpha_2 = 5.1 \pm 0.3$ near the MM-AI transition. All these features indicate that the MM phase prevails in ferromagnetic 2DEGs with SOIs and favors the exponential divergence of ξ at critical points.

TABLE I. Critical disorders $W_{c,1}$, exponents α_1, degrees of freedom N_f, and goodness of fit Q of the DM-MM transitions for different parameters.

	$W_{c,1}$	α_1	y	N_f	Q
$E = 0.2$, $\Delta = 0.005$	0.45 ± 0.01	12 ± 3	-2 ± 1	35	0.2
$E = 0.2$, $\Delta = 0.02$	0.28 ± 0.02	22 ± 3	-5 ± 2	30	0.2
$E = 0$, $\Delta = 0.005$	0.24 ± 0.01	7 ± 4	-0.7 ± 0.5	30	0.4

TABLE II. Critical disorders $W_{c,2}$, exponents α_2, degrees of freedom N_f, and goodness of fit Q of the MM-AI transitions for different parameters.

	$W_{c,2}$	α_2	y	N_f	Q
$E = 0.2, \Delta = 0.005$	0.47 ± 0.03	6 ± 4	-0.7 ± 0.3	25	0.4
$E = 0.2, \Delta = 0.02$	0.44 ± 0.05	6 ± 1	-2 ± 1	35	0.5
$E = 0, \Delta = 0.005$	0.28 ± 0.02	4 ± 2	-1.6 ± 0.9	30	0.8

IV. FRACTAL NATURE OF THE WAVE FUNCTION AND INVERSE PARTICIPATION RATIO

Having established the universality of DM-MM-AI transitions, we further consider the nature of wave functions in three phases, especially the fractal structure of wave functions in the MM phase. Wave functions at an isolated critical point of an ALT or in the critical band are known to have multifractal structures characterized by a set of anomalous dimensions measuring how their moments scale with sizes [12,21,35,43]. Among them, the fractal dimension is related to the IPR defined as

$$p_2(E, W) = \sum_i |\psi_i(E, W)|^4, \tag{6}$$

with $\psi_i(E, W)$ being the renormalized wave functions of energy E and disorder W at site i for a specific realization. For large enough systems, the average IPR scales with size L as [43–45]

$$p_2(E, W) \propto L^{-D}, \tag{7}$$

with D being the fractal dimension. If the state is extended (localized), $D = d$ ($D = 0$), where $d = 2$ is the spatial dimension. However, for a critical state, an anomalous scaling with L is expected, i.e., $D \in [0, d]$. Thus, we expect that states in the MM phase have a universal fractal dimension such that their wave functions occupy a sparse space.

Eigenfunctions of model (1) are obtained from the exact diagonalization method. Our numerical computation was done in PYTHON. We first use the KWANT package [46] to construct a Hamiltonian matrix H out of tight-binding model (1). We then solve the eigenequation $H\psi = E\psi$ using the SCIPY library [47] for various L ranging from 350 to 450. The average logarithms of IPR for state $E = 0.2$ [the same as in Fig. 2(a)] as a function of $\ln L$ for $W = 0.08$, 0.28, 0.42, 0.56, and 0.66 are shown in Fig. 5(a). The corresponding curves are virtually straight lines, which provide strong evidence of the scaling law Eq. (7). The slopes (fractal dimensions) clearly decrease with the increase of W from the DM phase to the AI phase, and $D = 1.90 \pm 0.02$ for $W_{c,1} < W = 0.42 < W_{c,2}$ in the MM phase.

We further authenticate the universality of the fractal nature by displaying $D(W)$ at $E = 0.2$ for a large range of disorders covering the three phases in Fig. 5(b). Apparently, a plateau of $D = 1.90$ is observed in the MM phase determined by data in Fig. 2(a), indicating that the fractal dimension of the fixed line does not depend on W. For $W < W_{c,1}$ (DM), wave functions are not a fractal anymore since $D \simeq d$, while, for $W \gg W_{c,2}$, IPRs are found to be independent of L, i.e., $D = 0$ [see the inset of Fig. 5(b)], a typical feature for AIs.

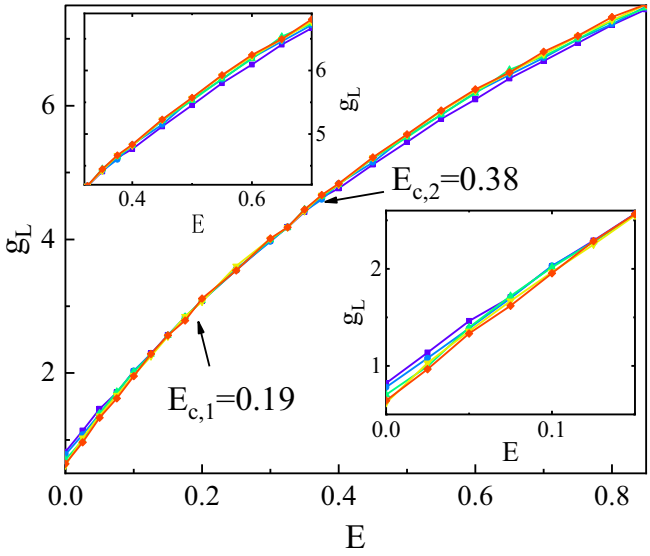

FIG. 4. g_L vs E for $W = 0.4$. $L = 128$ (purple), 192 (blue), 256 (green), 384 (yellow), and 512 (red). Here $\Delta = 0.01$, and $\tilde{\alpha} = 0.2$.

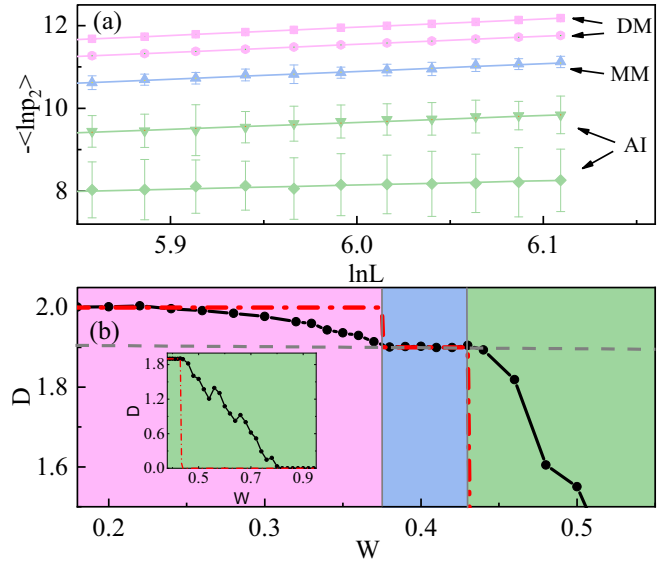

FIG. 5. (a) $-\langle \ln p_2 \rangle$ vs $\ln L$ for $E = 0.2$. Several disorders in different phases are chosen. DM: $W = 0.08$ (squares) and 0.28 (circles); MM: $W = 0.42$ (upward triangles); AI: $W = 0.56$ (downward triangles) and 0.66 (diamonds). Solid lines are linear fits of numerical data. (b) D as a function of W for $E = 0.2$ (circles). The dashed line shows the plateau of $D = 1.90$. The dot-dashed line is the schematic plot for $L \to \infty$. The three phases, colored magenta (DM), blue (MM), and green (AI), are identified according to data in Fig. 2.

TABLE III. Fractal dimensions D obtained from different ranges of L for some typical disorders.

	DM		MM		AI	
W	0.32	0.36	0.40	0.42	0.46	0.50
$L = 150$–250	1.93	1.91	1.89	1.90	1.89	1.85
$L = 200$–300	1.94	1.91	1.90	1.90	1.88	1.81
$L = 350$–450	1.96	1.93	1.90	1.90	1.82	1.78

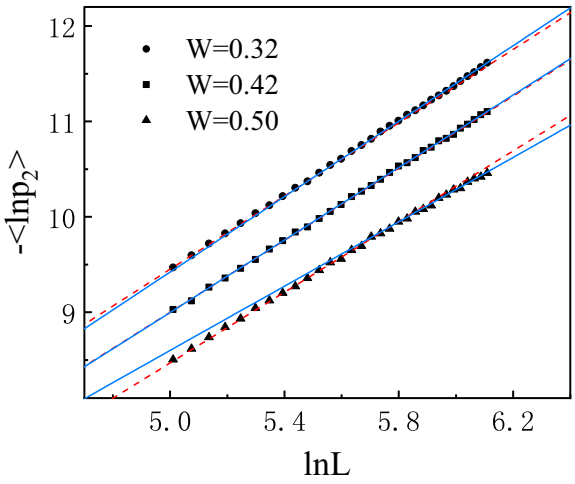

FIG. 6. $-\langle \ln p_2 \rangle$ vs $\ln L$ for $W = 0.32$ (the DM phase), $W = 0.42$ (the MM phase), and $W = 0.50$ (the AI phase). Other parameters are the same as in Fig. 2. For each disorder, solid and dashed lines are obtained by performing linear fits of data of $L = 350$ to 450 and $L = 150$ to 250, respectively, with slopes measuring the fractal dimensions.

We note that the dimension of those states in the DM (AI) regime near the phase transition point is not exactly $D = d = 2$ ($D = 0$) for $W < W_{c,1}$ ($W > W_{c,2}$). However, D become respectively larger and smaller for $W < W_{c,1}$ and $W > W_{c,2}$ when the system size increases, while D does not change with system size for $W \in [W_{c,1}, W_{c,2}]$, as demonstrated in Table III and Fig. 6. Naturally, we expect that D drops from 2 to 1.9 and from 1.9 to 0 at $W_{c,1}$ and $W_{c,2}$ under the thermodynamic limit of $L \to \infty$ [see the schematic plot in Fig. 5(b)]. Therefore, our calculations on the fractal dimensions, as additional evidence, support the existence of the marginal metals and the quantum phase transitions from the diffusive metals to the marginal metals and from the marginal metals to the Anderson insulators.

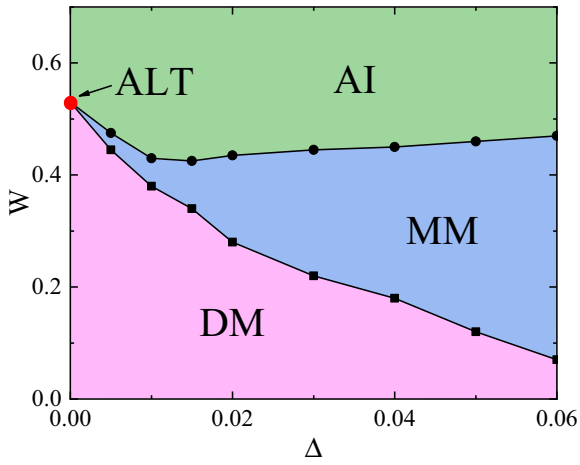

FIG. 7. Schematic phase diagram in the Δ-W plane: DM (magenta), MM (blue), and AI (green) at $E = 0.2$. Only an isolated critical level exists at $\Delta = 0$ (symplectic ensemble) with $\xi \propto |W - W_c|^{-\nu}$ and $\nu = 2.8 \pm 0.1$. For $\Delta \neq 0$, the MM phase exists within a window of $[W_{c,1}(\Delta), W_{c,2}(\Delta)]$, and ξ in the vicinity of $W_{c,1}$ (black squares) and $W_{c,2}$ (black circles) diverges exponentially as $\xi \propto \exp[\alpha/\sqrt{|W - W_c|}]$.

It is also enlightening to compare the fractal dimensions of the MM phase in model (1) with those of critical states in other 2D materials. The fractal dimension of isolated critical levels for ALTs in the symplectic ensemble is found to be 1.66 ± 0.05 [48], while $D = 1.75$ for the quantum Hall-type criticality [49]. Thus, wave functions in the MM phase with $D = 1.90 \pm 0.02$ are more packed than those critical states of the random SU(2) model under strong magnetic fields [21].

A more inclusive picture is procured by exhaustive simulations of different Δ and the same $E = 0.2$. The fixed line persists at finite Δ as expected, such that the three phases coexist, and model (1) always experiences the DM-MM-AI phase transitions at Δ-dependent transition points $W_{c,1}$ and $W_{c,2}$. However, for $\Delta = 0$, there is only one quantum critical state at which the system undergoes a normal ALT. Furthermore, it is numerically justified that the correlation lengths ξ always diverge as $\xi \propto \exp[\alpha/\sqrt{|W - W_c|}]$ near $W_{c,1}$ (squares) and $W_{c,2}$ (circles) in Fig. 7.

V. SUMMARY

In conclusion, the dimensionless conductance and the IPR provide substantial evidence of the existence of a marginal-metallic phase between a diffusive-metal phase and an Anderson insulator phase in ferromagnetic 2DEGs with SOIs. Such systems undergo a DM-MM-AI transition as either disorder strength or Fermi level varies. Near the transition points, the conductance can be described well by the one-parameter scaling hypothesis. The criticality of the DM-MM-AI transitions is consistent with the notion of universality of a quantum phase transition in the sense that correlation lengths diverge exponentially with the inverse square root of $|W - W_c|$ for all critical points. In addition, eigenfunctions in the MM phase are of fractals of dimension $D = 1.90$, while extended states in the DM phase spread over the entire lattice. A schematic phase diagram in the Δ-W plane was presented.

The physical mechanism behind the marginal metal phase is still an open question and deserves further study. However, we notice that such two-step quantum phase transitions of KT type can occur in some 2D spinful systems driven by thermal spin fluctuations, e.g., the six-clock model [50]. More interestingly, such a two-step KT-type phase transition was also reported in the quantum anomalous Hall system [51] recently, but the MM phase is separated by two insulating phases: The normal insulator and the Chern insulator.

ACKNOWLEDGMENTS

We are grateful to C. Chen and H. Jiang for valuable discussions. This work is supported by the National Key Research and Development Program of China (Grant No. 2016YFA0200604), the National Natural Science Foundation of China (Grants No. 11774296, No. 11704061, No. 21873088, No. 11974296, and No. 11874337), and Hong Kong RGC (Grants No. 16301518 and No. 16301619). C.W. is supported by UESTC and the China Postdoctoral Science Foundation (Grants No. 2017M610595 and

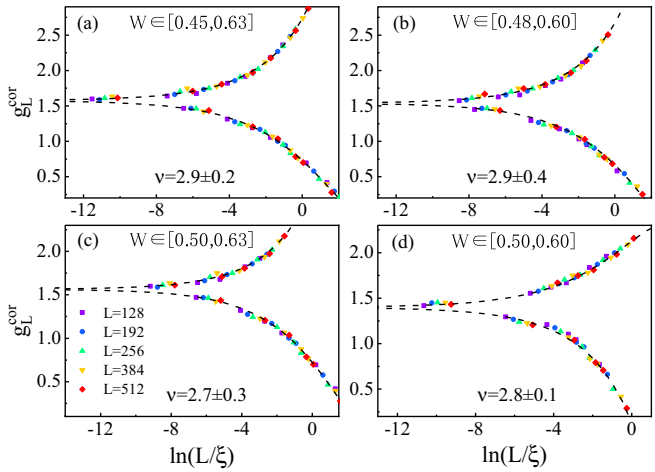

FIG. 8. Scaling function $f(x = \ln(L/\xi))$ for $E = 0.2$ and $\Delta = 0$ (GSE).

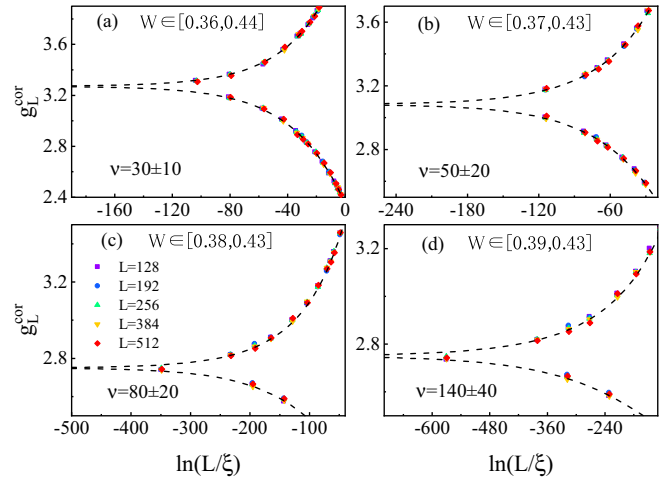

FIG. 9. Scaling functions $f(x = \ln(L/\xi))$ based on the hypothesis of the Anderson localization transition (single fixed point W_c and correlation lengths diverging as a power law $\xi \propto |W - W_c|^{-\nu}$) for $E = 0.2$, $\Delta = 0.01$, and different ranges of disorder: (a) $W \in [0.36, 0.44]$, (b) $W \in [0.37, 0.43]$, (c) $W \in [0.38, 0.43]$, and (d) $W \in [0.39, 0.43]$.

No. 2017T100684). C.W. also acknowledges the support from P. Yan and X. Wang.

APPENDIX: ONE-PARAMETER SCALING ANALYSIS

The one-parameter scaling hypothesis claims that near the quantum phase transition points the dimensionless conductance is a function of a single parameter, $x = L/\xi$ [Eq. (5)], i.e., $g_L = f(L/\xi)$, with L being the system size and ξ being the correlation length and diverging at the critical point. However, previous numerical studies suggested that irrelevant scaling variables, as well as the nonlinearity of the scaling variables, can play a significant role in the finite-size scaling analysis [42] when the system size is not large enough. We therefore follow the proved method in the literature [42] and carry out finite-size scaling analysis by including irrelevant scaling variable ϕ (up to the first order):

$$g_L = f(L/\xi) + \phi L^y \tilde{f}(L/\xi), \tag{A1}$$

where $y < 0$ is the exponent of the irrelevant variable. We expand $f(x)$ and $\tilde{f}(x)$ as

$$\begin{aligned} f(L/\xi) &= g_c + (L/\xi)^{1/\nu} + a_1(L/\xi)^{2/\nu}, \\ \tilde{f}(L/\xi) &= a_2 + (L/\xi)^{1/\nu} + a_3(L/\xi)^{2/\nu}. \end{aligned} \tag{A2}$$

Here ϕ, y, ν, g_c, a_1, a_2, a_3 are fitting parameters.

If the system undergoes an ALT at a critical disorder $W = W_c$, the correlation length diverges as

$$\xi = (b_1 w + b_2 w^2)^{-\nu}, \tag{A3}$$

where $w = |W - W_c|/W_c$ and $b_{1,2}$ are extra fitting parameters. By performing a χ^2 fit of the $g_L(W)$ numerically obtained with Eqs. (A2) and (A3) (we use the nonlinear surface fit of ORIGINPRO [52]), we can calculate the critical disorder W_c and the critical exponent ν for a given set of parameters, e.g., the Fermi energy E, the Rashba SOI $\tilde{\alpha}$, and the ferromagnetic coupling Δ. In our analysis we use the percentile conductances of $q = 0.5$ [53] to estimate the likely accuracy of conductances.

Let us consider the case of $\Delta = 0$ (GSE) shown in the inset of Fig. 2(a) as one example. The χ^2 fit yields $W_c = 0.53 \pm 0.01$, $\nu = 2.8 \pm 0.1$, $g_c = 1.40 \pm 0.01$, $\phi = -0.22 \pm 0.06$, $y = -1.5 \pm 0.3$, $a_1 = -0.27 \pm 0.02$, $a_2 = -120 \pm 20$, $a_3 = 670 \pm 60$, $b_1 = -1.25 \pm 0.02$, and $b_2 = 3 \pm 1$ for $W \in [0.50, 0.60]$. We plot the scaling function by subtracting the correction of the one-parameter scaling hypothesis,

$$g_L^{cor} = g_L - \phi L^y \tilde{f}(L/\xi), \tag{A4}$$

and use g_L^{cor} to obtain the β function:

$$\beta = \frac{d \ln g_L^{cor}}{d \ln L} \approx \frac{1}{g_L^{cor}} \frac{1}{\nu} \left(\frac{L}{\xi}\right)^{1/\nu} \approx \frac{1}{\nu}\left(\ln g_L^{cor} - \ln g_c\right), \tag{A5}$$

as shown in Fig. 1 (the red line). Our numerical calculations yield a universal critical exponent of $\nu \simeq 2.8 \pm 0.1$,

TABLE IV. Correlation length exponents (ν and y), critical disorders W_c, degrees of freedom N_f, and goodness of fit Q for different ranges of disorders and $E = 0.2$ and $\Delta = 0$.

Range of disorders	ν	W_c	y	N_f	Q
$W \in [0.45, 0.63]$	2.9 ± 0.2	0.53 ± 0.01	-2.4 ± 0.8	60	0.3
$W \in [0.48, 0.60]$	2.9 ± 0.4	0.53 ± 0.01	-1.6 ± 0.9	50	0.2
$W \in [0.50, 0.63]$	2.7 ± 0.3	0.53 ± 0.01	-2.1 ± 0.8	50	0.6
$W \in [0.50, 0.60]$	2.8 ± 0.1	0.53 ± 0.01	-1.5 ± 0.3	45	0.7

TABLE V. Correlation length exponents (ν and y), critical disorders W_c, degrees of freedom N_f, and goodness of fit Q for different ranges of disorders and $E = 0.2$ and $\Delta = 0.01$.

Range of disorders	ν	W_c	y	N_f	Q
$W \in [0.36, 0.44]$	30 ± 10	0.39 ± 0.09	-1.2 ± 0.9	100	0.2
$W \in [0.37, 0.43]$	50 ± 20	0.40 ± 0.01	-5.0 ± 0.5	65	0.4
$W \in [0.38, 0.43]$	80 ± 20	0.42 ± 0.02	-2.5 ± 0.7	55	0.5
$W \in [0.39, 0.43]$	140 ± 40	0.42 ± 0.08	-2 ± 1	40	0.5

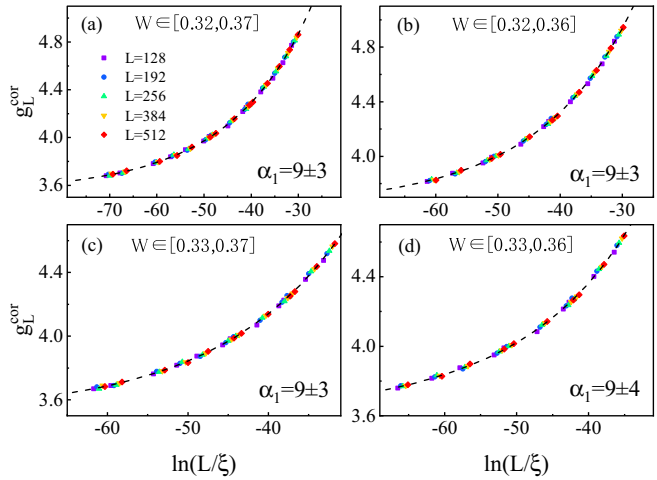

FIG. 10. Scaling functions $f(x = \ln(L/\xi))$ assuming correlation lengths diverging as $\xi \propto \exp[\alpha_1/\sqrt{W - W_{c,1}}]$ in the DM phase closed to the phase transition points. Here $E = 0.2$, and $\Delta = 0.01$, with different ranges of disorders: (a) $W \in [0.32, 0.37]$, (b) $W \in [0.32, 0.36]$, (c) $W \in [0.33, 0.37]$, and (d) $W \in [0.33, 0.36]$.

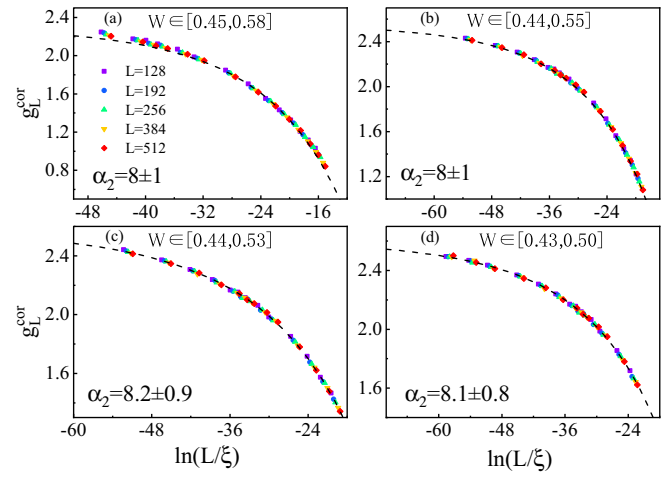

FIG. 11. Scaling functions $f(x = \ln(L/\xi))$ by assuming correlation lengths diverging as $\xi \propto \exp[\alpha_2/\sqrt{W - W_{c,2}}]$ in the AI phase closed to the phase transition points. Here $E = 0.2$, and $\Delta = 0.01$, with different ranges of disorders: (a) $W \in [0.45, 0.58]$, (b) $W \in [0.44, 0.55]$, (c) $W \in [0.44, 0.53]$, and (d) $W \in [0.43, 0.50]$.

independent of the range of disorders, as shown in Fig. 8 and in Table IV.

For $\Delta \neq 0$, we first carry out the finite-size scaling analysis by assuming only one quantum phase transition point for the data presented in Fig. 2(a). We further assume that the correlation length ξ diverges as a power law $\xi \propto |W - W_c|^{-\nu}$. Under these assumptions, the obtained critical exponent ν dramatically increases from 30 to 140 when data closer to the transition point are used (see Fig. 9 and Table V). Therefore, our finite-size scaling analysis excludes the possibility of the single quantum phase transition.

We thus assume that for $\Delta \neq 0$ the system undergoes two quantum phase transitions. One is from DMs to MMs, and the other is from MMs to AIs as the disorder strength increases. The scaling function that expands in terms of the irrelevant variable ϕ up to first order is

$$g_L = g_c + c_1\left(\frac{L}{\xi}\right)^u + c_2\left(\frac{L}{\xi}\right)^{2u} + \phi L^y\left[1 + c_3\left(\frac{L}{\xi}\right)^u + c_4\left(\frac{L}{\xi}\right)^{2u}\right], \quad \text{(A6)}$$

similar to Eq. (A1), but with an exponentially diverging correlation length, $\xi = \exp[\alpha/\sqrt{|W - W_c|}]$. Here $g_c, W_c, u, \alpha, \phi, y, c_1, c_2, c_3, c_4$ are the fitting parameters. Following the same procedures as those for the ALTs explained earlier, we can obtain all the parameters, including the critical disorder W_c and α.

Taking data in Fig. 3 as an example, we obtain $W_{c,1} = 0.38 \pm 0.01$, $\alpha_1 = 9 \pm 4$, $g_c = 3.5 \pm 0.5$, $\phi = 0.25 \pm 0.03$, $y = -0.7 \pm 0.5$, $u = 0.05 \pm 0.03$, $c_1 = 3.5 \pm 0.2$, $c_2 = 9.1 \pm 0.5$, $c_3 = -110 \pm 20$, and $c_4 = 520 \pm 50$ for the DM-MM transition and $W_{c,2} = 0.43 \pm 0.01$, $\alpha_2 = 8 \pm 1$, $g_c = 2.6 \pm 0.2$, $\phi = 9 \pm 1$, $y = -1.2 \pm 0.4$, $u = 0.05 \pm 0.01$, $c_1 = -2.0 \pm 0.3$, $c_2 = -3.5 \pm 0.6$, $c_3 = -6.4 \pm 0.7$, and $c_4 = 6.8 \pm 0.4$ for the MM-AI transition. As before, the corrected conductance can be obtained with

$$g_L^{\rm cor} = g_L - \phi L^y\left[1 + c_3\left(\frac{L}{\xi}\right)^u + c_4\left(\frac{L}{\xi}\right)^{2u}\right]. \quad \text{(A7)}$$

Figures 10 and 11 show the scaling functions obtained by collapsing all $g_L^{\rm cor}$ for different sizes L near $W_{c,1}$ (DM to MM) and $W_{c,2}$ (MM to AI) into a single curve. Since $g_L^{\rm cor}$ is obtained from the raw numerical data by subtracting contributions from the irrelevant variable that are given by the fitting parameters, it is important that the final results do not vary with the data sets used. Indeed, our scaling functions for both the DM and AI phases do not depend on the ranges of disorders used (see Table VI), which is strong support for the hypothesis of two quantum phase transitions.

TABLE VI. Correlation length exponents (α_1, α_2), critical disorders ($W_{c,1}, W_{c,2}$), degrees of freedom N_f, and goodness of fit Q for different ranges of disorders and $E = 0.2$ and $\Delta = 0.01$.

Diffusive metals to marginal metals						Marginal metals to Anderson insulators					
Range of disorders	α_1	$W_{c,1}$	y	N_f	Q	Range of disorders	α_2	$W_{c,2}$	y	N_f	Q
$W \in [0.32, 0.37]$	9 ± 3	0.39 ± 0.01	-0.3 ± 0.1	60	0.3	$W \in [0.45, 0.58]$	8 ± 1	0.43 ± 0.06	-1.5 ± 0.3	65	0.4
$W \in [0.32, 0.36]$	9 ± 3	0.38 ± 0.01	-0.2 ± 0.1	45	0.2	$W \in [0.44, 0.55]$	8 ± 1	0.43 ± 0.01	-1.2 ± 0.4	65	0.6
$W \in [0.33, 0.37]$	9 ± 3	0.39 ± 0.01	-0.3 ± 0.2	50	0.5	$W \in [0.44, 0.53]$	8.2 ± 0.9	0.42 ± 0.01	-1.2 ± 0.6	55	0.4
$W \in [0.33, 0.36]$	9 ± 4	0.38 ± 0.01	-0.7 ± 0.5	40	0.5	$W \in [0.43, 0.50]$	8.1 ± 0.8	0.42 ± 0.01	-1.3 ± 0.5	55	0.5

The corresponding β function in both the DM and AI phases is

$$\beta = \frac{1}{g_L^{\rm cor}}\left[uc_1\left(\frac{L}{\xi}\right)^u + 2uc_2\left(\frac{L}{\xi}\right)^{2u}\right], \tag{A8}$$

and

$$\beta = 0 \tag{A9}$$

in the MM phase since $\xi = +\infty$. For large g_L, we assume the following analytical expression:

$$\beta = f_1 g_L^{-1} + f_4 g_L^{-4} + o\left(g_L^{-5}\right), \tag{A10}$$

where f_1 and f_4 are fitting parameters. When $f_1 = 1/\pi$ and $f_4 = -3\zeta(3)/4$ [$\zeta(x)$ is the Riemann zeta function], this is the β function of the 2D GUE obtained from the nonlinear σ model [15]. We use Eqs. (A8), (A9), and (A10) to draw the β function in Fig. 1 (the black line).

[1] P. W. Anderson, Absence of diffusion in certain random lattices, Phys. Rev. **109**, 1492 (1958).

[2] S. John, Electromagnetic Absorption in a Disordered Medium near a Photon Mobility Edge, Phys. Rev. Lett. **53**, 2169 (1984).

[3] P. Sheng and Z.-Q. Zhang, Scalar-Wave Localization in a Two-Component Composite, Phys. Rev. Lett. **57**, 1879 (1986).

[4] D. S. Wiersma, P. Bartolini, A. Lagendijk, and R. Righini, Localization of light in a disordered medium, Nature (London) **390**, 671 (1997).

[5] M. Störzer, P. Gross, C. M. Aegerter, and G. Maret, Observation of the Critical Regime near Anderson Localization of Light, Phys. Rev. Lett. **96**, 063904 (2006).

[6] A. A. Chabanov, M. Stoytchev, and A. Z. Genack, Statistical signatures of photon localization, Nature (London) **404**, 850 (2000).

[7] H. Hu, A. Strybulevych, J. H. Page, S. E. Skipetrov, and B. A. van Tiggelen, Localization of ultrasound in a three-dimensional elastic network, Nat. Phys. **4**, 945 (2008).

[8] T. Schwartz, G. Bartal, S. Fishman, and M. Segev, Transport and Anderson localization in disordered two-dimensional photonic lattices, Nature (London) **446**, 52 (2007).

[9] C. Wang, Y. Cao, X. R. Wang, and P. Yan, Interplay of wave localization and turbulence in spin Seebeck effect, Phys. Rev. B **98**, 144417 (2018).

[10] P. A. Lee and T. V. Ramakrishnan, Disordered electronic systems, Rev. Mod. Phys. **57**, 287 (1985).

[11] B. Kramer and A. MacKinnon, Localization: Theory and experiment, Rep. Prog. Phys. **56**, 1469 (1993).

[12] F. Evers and A. D. Mirlin, Anderson transitions, Rev. Mod. Phys. **80**, 1355 (2008).

[13] E. Abrahams, P. W. Anderson, D. C. Licciardello, and T. V. Ramakrishnan, Scaling Theory of Localization: Absence of Quantum Diffusion in Two Dimensions, Phys. Rev. Lett. **42**, 673 (1979).

[14] D. Friedan, Nonlinear Models in $2+\epsilon$ Dimensions, Phys. Rev. Lett. **45**, 1057 (1980).

[15] S. Hikami, Localization, Nonlinear σ model and string theory, Prog. Theor. Phys. Suppl. **107**, 213 (1992).

[16] S. N. Evangelou, Anderson Transition, Scaling, and Level Statistics in the Presence of Spin Orbit Coupling, Phys. Rev. Lett. **75**, 2550 (1995).

[17] R. Merkt, M. Janssen, and B. Huckestein, Network model for a two-dimensional disordered electron system with spin-orbit scattering, Phys. Rev. B **58**, 4394 (1998).

[18] Y. Asada, K. Slevin, and T. Ohtsuki, Anderson Transition in Two-Dimensional Systems with Spin-Orbit Coupling, Phys. Rev. Lett. **89**, 256601 (2002).

[19] P. Markoš and L. Schweitzer, Critical regime of two-dimensional Ando model: Relation between critical conductance and fractal dimension of electronic eigenstates, J. Phys. A **39**, 3221 (2006).

[20] G. Orso, Anderson Transition of Cold Atoms with Synthetic Spin-Orbit Coupling in Two-Dimensional Speckle Potentials, Phys. Rev. Lett. **118**, 105301 (2017).

[21] C. Wang, Y. Su, Y. Avishai, Y. Meir, and X. R. Wang, Band of Critical States in Anderson Localization in a Strong Magnetic Field with Random Spin-Orbit Scattering, Phys. Rev. Lett. **114**, 096803 (2015).

[22] Y. Su, C. Wang, Y. Avishai, Y. Meir, and X. R. Wang, Absence of localization in disordered two-dimensional electron gas at weak magnetic field and strong spin-orbit coupling, Sci. Rep. **6**, 33304 (2016).

[23] C. Wang and X. R. Wang, Anderson transition of two-dimensional spinful electrons in the Gaussian unitary ensemble, Phys. Rev. B **96**, 104204 (2017).

[24] D. J. Thouless, M. Kohmoto, M. P. Nightingale, and M. den Nijs, Quantized Hall Conductance in a Two-Dimensional Periodic Potential, Phys. Rev. Lett. **49**, 405 (1982).

[25] A. M. M. Pruisken, Universal Singularities in the Integral Quantum Hall Effect, Phys. Rev. Lett. **61**, 1297 (1988).

[26] B. Huckestein, Scaling theory of the integer quantum Hall effect, Rev. Mod. Phys. **67**, 357 (1995).

[27] D. C. Tsui, H. L. Stormer, and A. C. Gossard, Two-Dimensional Magnetotransport in the Extreme Quantum Limit, Phys. Rev. Lett. **48**, 1559 (1982).

[28] R. B. Laughlin, Anomalous Quantum Hall Effect: An Incompressible Quantum Fluid with Fractionally Charged Excitations, Phys. Rev. Lett. **50**, 1395 (1983).

[29] R. Sepehrinia, Universality of Anderson transition in two-dimensional systems of symplectic symmetry class, Phys. Rev. B **81**, 045104 (2010).

[30] Y. Su and X. R. Wang, Role of spin degrees of freedom in Anderson localization of two-dimensional particle gases with random spin-orbit interactions, Phys. Rev. B **98**, 224204 (2018).

[31] X. C. Xie, X. R. Wang, and D. Z. Liu, Kosterlitz-Thouless-Type Metal-Insulator Transition of a 2D Electron Gas in a Random Magnetic Field, Phys. Rev. Lett. **80**, 3563 (1998).

[32] G. Xiong, S.-D. Wang, Q. Niu, D.-C. Tian, and X. R. Wang, Metallic Phase in Quantum Hall Systems due to Inter-Landau-Band Mixing, Phys. Rev. Lett. **87**, 216802 (2001).

[33] Y. Avishai and Y. Meir, New Spin-Orbit-Induced Universality Class in the Integer Quantum Hall Regime, Phys. Rev. Lett. **89**, 076602 (2002).

[34] J. Bang and K. J. Chang, Localization and one-parameter scaling in hydrogenated graphene, Phys. Rev. B **81**, 193412 (2010).
[35] Y.-Y. Zhang, J. Hu, B. A. Bernevig, X. R. Wang, X. C. Xie, and W. M. Liu, Localization and the Kosterlitz-Thouless Transition in Disordered Graphene, Phys. Rev. Lett. **102**, 106401 (2009).
[36] Y. Asada, K. Slevin, and T. Ohtsuki, Numerical estimation of the β function in two-dimensional systems with spin-orbit coupling, Phys. Rev. B **70**, 035115 (2004).
[37] J. H. Bardarson, J. Tworzydło, P. W. Brouwer, and C. W. J. Beenakker, One-Parameter Scaling at the Dirac Point in Graphene, Phys. Rev. Lett. **99**, 106801 (2007).
[38] Z. Xu, L. Sheng, R. Shen, B. Wang, and D. Y. Xing, Kosterlitz-Thouless transition in disordered two-dimensional topological insulators, J. Phys.: Condens. Matter **25**, 065501 (2013).
[39] N. Nagaosa, J. Sinova, S. Onoda, A. H. MacDonald, and N. P. Ong, Anomalous Hall effect, Rev. Mod. Phys. **82**, 1539 (2010).
[40] A. MacKinnon, The calculation of transport properties and density of states of disordered solids, Z. Phys. B **59**, 385 (1985).
[41] S. Datta, *Electronic Transport in Mesoscopic Systems* (Cambridge University Press, Cambridge, 1995).
[42] K. Slevin and T. Ohtsuki, Corrections to Scaling at the Anderson Transition, Phys. Rev. Lett. **82**, 382 (1999).
[43] X. R. Wang, Y. Shapir, and M. Rubinstein, Analysis of multiscaling structure in diffusion-limited aggregation: A kinetic renormalization-group approach, Phys. Rev. A **39**, 5974 (1989).
[44] M. Janssen, Statistics and scaling in disordered mesoscopic electron systems, Phys. Rep. **295**, 1 (1998).
[45] J. H. Pixley, P. Goswami, and S. Das Sarma, Anderson Localization and the Quantum Phase Diagram of Three Dimensional Disordered Dirac Semimetals, Phys. Rev. Lett. **115**, 076601 (2015).
[46] C. W. Groth, M. Wimmer, A. R. Akhmerov, and X. Waintal, Kwant: A software package for quantum transport, New J. Phys. **16**, 063065 (2014).
[47] E. Jones, E. Oliphant, P. Peterson *et al.*, SCIPY, open source scientific tools for PYTHON, http://www.scipy.org/.
[48] H. Obuse and K. Yakubo, Anomalously localized states and multifractal correlations of critical wave functions in two-dimensional electron systems with spin-orbital interactions, Phys. Rev. B **69**, 125301 (2004).
[49] F. Evers, A. Mildenberger, and A. D. Mirlin, Multifractality at the spin quantum Hall transition, Phys. Rev. B **67**, 041303(R) (2003).
[50] T. Surungan and Y. Okabe, Kosterlitz-Thouless transition in planar spin models with bond dilution, Phys. Rev. B **71**, 184438 (2005).
[51] C. Z. Chen, H. Liu, and X. C. Xie, Effects of Random Domains on the Zero Hall Plateau in the Quantum Anomalous Hall Effect, Phys. Rev. Lett. **122**, 026601 (2019).
[52] ORIGINPRO, version 2019b, OriginLab Corporation, Northampton, MA, 2019.
[53] K. Slevin, P. Markoš, and T. Ohtsuki, Scaling of the conductance distribution near the Anderson transition, Phys. Rev. B **67**, 155106 (2003).